Osteopontin attenuates secondary neurodegeneration in the thalamus after experimental stroke

Anne Ladwig[1*], Rebecca Rogall[1*], Jörg Hucklenbroich[1], Antje Willuweit[3], Michael Schoeneck[3], Karl-Josef Langen[3], Gereon R. Fink[1,2], M. Adele Rueger[1,2], Michael Schroeter[1,2]

[1]Dept. of Neurology, University Hospital Cologne, Cologne, Germany

[2]INM-3 and [3]INM-4, Research Centre Juelich, Juelich, Germany

*The two first authors (Anne Ladwig and Rebecca Rogall) contributed equally to this work.

Corresponding author:

Department of Neurology

University Hospital of Cologne

Kerpener Strasse 62

50924 Cologne, Germany

Phone: +49-221-478-32028

Fax: +49-221-478-89143

Email:

Abstract

Cortical cerebral ischemia elicits neuroinflammation as well as secondary neuronal degeneration in remote areas. Locally distinct and specific secondary neurodegeneration affecting thalamic nuclei connected to cortical areas highlights such processes. Osteopontin (OPN) is a cytokine-like glycoprotein that is excreted in high amounts after cerebral ischemia and exerts various immunomodulatory functions. We here examined putative protective effects of OPN in secondary thalamic degeneration. We subjected male Wistar rats to photothrombosis and subsequently injected OPN or placebo intracerebroventricularly. Immunohistochemical and fluorescence staining was used to detect the extent of neuronal degeneration and microglia activation. *Ex vivo* autoradiography with radiotracers available for human *in vivo* PET studies, i.e., CIS-4-[^{18}F]Fluor-D-Proline (D-cis-[^{18}F]FPRO), and [6-^{3}H]thymidine ([^{3}H]thymidine), confirmed degeneration and proliferation, respectively.

We found secondary neurodegeneration in the thalamus characterized by microglial activation and neuronal loss. Neuronal loss was restricted to areas of microglial infiltration. Treatment with OPN significantly decreased neurodegeneration, inflammation and microglial proliferation. Microglia displayed morphological signs of activation without expressing markers of M1 or M2 polarization. D-CIS-[^{18}F]FPRO-uptake mirrored attenuated degeneration in OPN-treated animals. Notably, [^{3}H]thymidine and BrdU-staining revealed increased stem cell proliferation after treatment with OPN.

The data suggest that OPN is able to ameliorate secondary neurodegeneration in thalamic nuclei. These effects can be visualized by radiotracers D-CIS-[^{18}F]FPRO and [^{3}H]thymidine, opening new vistas for translational studies.

213 *words*

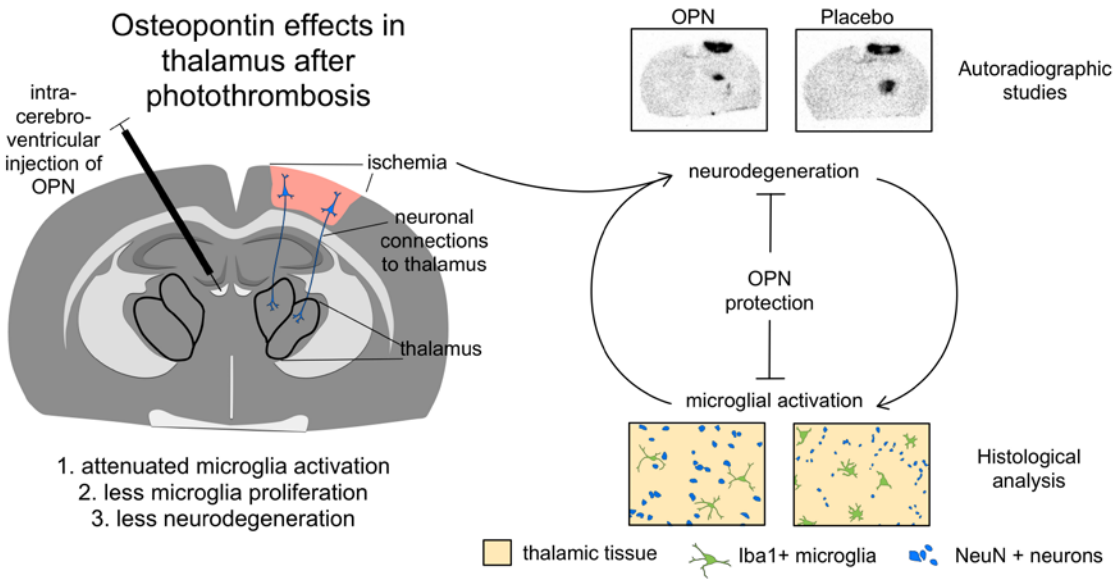

Graphical abstract

Keywords
Osteopontin; stroke; secondary neurodegeneration; neuroinflammation; microglia, autoradiography

1. Introduction

Cerebral ischemia causes neuroinflammation not only in the primary region of the insult but also in remote areas such as the thalamus (Myers et al. 1991; Ogawa et al. 1997; Stoll et al. 1998; Schroeter et al. 2006; Walberer et al. 2010). Spatially distinct from the ischemic injury, thalamic microglia activation delineates secondary neurodegeneration of distinct thalamic nuclei dependent upon specific projections from the area of the primary insult (Myers et al. 1991; Pappata et al. 2000). Such thalamic neurodegeneration contributes to the persisting clinical deficits (Freret et al. 2006; De Vloo et al. 2017). Importantly, microglia activation may sustain disease progression. Inflammatory mediators produced from classically polarized microglia (M1) result in an exacerbation of tissue damage (Kanazawa et al. 2017). In stark contrast, however, anti-inflammatory mediators released from alternatively polarized microglia (M2) can also assert protective functions (Xiong et al. 2016; Orihuela et al. 2016). Modulating this immune response holds promise to attenuate secondary cell damage after cerebral ischemia (Xia et al. 2015).

The acidic phosphoglycoprotein Osteopontin (OPN) is robustly induced in response to tissue injury and inflammation (Butler 1989, 1995; Giachelli et al. 1995; Denhardt et al. 2001; Fu et al. 2012; Morales-Ibanez et al. 2013; Kato et al. 2014). OPN is involved in angiogenesis, wound healing, tissue homeostasis, as well as the immune response (McKee and Nanci 1996;

Myles and Leung 2008; Wang and Denhardt 2008; Kumar et al. 2013). OPN is constitutively expressed in the brain (Ellison et al. 1998) and - in the subacute stage of cerebral ischemia - OPN is upregulated in microglia and macrophages in the infarct zone and peri-infarct regions (Wang et al. 1998; Ellison et al. 1998; Lee et al. 1999; Hedtjärn et al. 2004; Hur et al. 2007; Wang and Denhardt 2008; Ladwig et al. 2017). OPN knockout studies suggest a direct neuroprotective effect of OPN on neurons (Meller et al. 2005; Doyle et al. 2008) and an indirect neuroprotective effect via regulation of the microglial response, namely inducible nitric oxide synthase (iNOS) production (Schroeter et al. 2006). Increased neurodegeneration in OPN-deficient mice with an excitotoxic corticostriatal lesion mirrors the described protective effects of OPN (Meller et al. 2005; Schroeter et al. 2006; Doyle et al. 2008). Furthermore, we recently observed that OPN increases proliferation and survival of neural stem cells (NSC) *in vitro* (Rabenstein et al. 2015), and polarizes microglia towards an anti-inflammatory phenotype (Rabenstein et al. 2016). Based on the studies mentioned above, we hypothesized that OPN modulates microglia activation thereby attenuating secondary thalamic degeneration.

To visualize both neurodegeneration and the attenuation of microglia activation we used *ex vivo* autoradiography and radiotracers that are also available for human studies with positron emission tomography (PET). Firstly, the tracer CIS-4-[^{18}F]fluoro-D-Proline (D-cis-[^{18}F]FPRO) readily crosses the blood-brain barrier and visualizes secondary neurodegeneration throughout various CNS pathologies (Langen et al. 2007). Secondly, the PET tracer and thymidine analog 3'-deoxy-3'-[^{18}F]fluoro-L-thymidine ([^{18}F]FLT) is trapped in proliferating cells (Rueger et al. 2010). We hypothesized that attenuating microglial activation via OPN is reflected by reduced local proliferation. For the sake of spatial resolution of thalamic subregions, we choose *ex vivo* autoradiography rather than *in vivo* PET and used [^{3}H]thymidine to visualize proliferation.

2. Material and methods

2.1 Animals and surgery

All animal procedures followed the German Laws of Animal Protection after obtaining the approval of the local animal care committee governmental authority.

2.1.1 Photothrombosis

Adult male Wistar rats (n = 16) weighing 200-300 g were fixated on a stereotactic frame after having been sedated with isoflurane (induction with 5 %, maintenance with 1,5%) and anesthetized with intraperitoneal (i.p.) ketamine (75 mg/kg) and medetomidine (0.5 mg/kg). Throughout surgical procedures, there was constant monitoring of pulse and oxygenation, the body temperature was maintained at 37.0°C with a thermostatically controlled heating pad.

Local cerebral ischemia was induced via photothrombosis as previously described (Ladwig et al. 2017). Shortly, in isoflurane-anesthetized spontaneously breathing rats, at the stereotactic coordinates 2.0 mm posterior and 3.0 mm lateral from bregma, a fiberoptic bundle of a cold light source with an aperture of 1.5 mm was placed onto the skull. The skull was illuminated for 20 minutes by a white light beam (150 W). The 1% dye rose bengal (Sigma, Munich, Germany) was injected intravenously (i.v.) in a concentration of 1 µg/g body weight before illumination. This procedure resulted in a cortical lesion of reproducible size (cf. Fig.1).

2.1.2 OPN treatment

During the same anesthesia, immediately after induction of photothrombosis, animals were randomly assigned to the treatment groups and injected with a single intracerebroventricular (i.c.v.) dose of either 500 µg recombinant OPN (R&D Systems, Minneapolis, USA) in 5 µl saline (n = 8), or 5 µl saline as control (placebo-group, n = 8) using the stereotactic coordinates bregma anterior-posterior -0.9 mm, medio-lateral +1.4 mm, ventro-dorsal +3.8 mm.

2.1.3 BrdU injections

To assess cell proliferation 5-Bromo-2'-deoxyuridine (BrdU; Sigma-Aldrich, Munich, Germany) was injected intraperitoneally in all 16 animals. Starting one day after photothrombosis, BrdU was injected four times in total, every second day at a concentration of 50 mg/kg. This regime resulted in a cumulative dose of 200 mg/kg BrdU per animal.

2.1.4 Double tracer ex vivo autoradiography

The synthesis of D-CIS-[^{18}F]FPRO was performed as described previously (Langen et al. 2007). [^{3}H]thymidine was obtained commercially (Perkin- Elmer, Waltham, MA, USA) as an aqueous solution with a specific activity of 533 GBq/mmol and a concentration of 37 MBq/mL. To examine the effect of OPN on cell proliferation, respectively activation of stem cells, 600 µCi of [^{3}H]thymidine and on secondary neurodegeneration ~50 MBq of D-CIS-[^{18}F]FPRO were injected into the tail vein under sedation with isoflurane 7, respectively 8 days after infarct induction. Two hours after the D-CIS-[^{18}F]FPRO injection the rats were sacrificed under deep anesthesia and the brains were removed immediately. Brains were subsequently frozen in 2-methylbutane, and serial coronal brain sections of 20 µm thickness were cut on a cryostat (CM3050S, Leica Microsystems, Wetzlar, Germany). Every tenth slide was kept for the autoradiograms. The remaining parallel brain sections were stored at -80 ºC for histologic staining and immunostaining. To quantify the tracer uptake in brain tissue, in-house calibrated chicken liver standards with a known concentration of D-CIS-[^{18}F]FPRO were produced and cut in the same manner as the brains. Brain slides were co-exposed with standards on a coated Phosphor imaging plate (Fuji BAS-TR 2025 SR, GE Life Sciences) over night. For [^{3}H]thymidine evaluation slides were exposed on uncoated phosphor imaging plates (Fuji BAS-TR 2025, GE Life Sciences) after the total decay of D-CIS-[^{18}F]FPRO for three days. To

quantify the thymidine uptake, commercial ^{3}H-standards (Microscales; Amersham Biosciences, Little Chalfont, UK) were co-exposed with the slides on the same plate. Imaging plates were scanned in a Fuji BAS-Reader at the highest resolution (25 µm), and quantitative autoradiograms were generated (in Bq/g tissue wet weight) via AIDA Image Analyzer software (Raytest Isotopenmessgeräte, Straubenhardt, Germany).

2.2 Histology and immunohistochemistry

To assess the patterns of microglia activation as well as secondary neurodegeneration in the thalamus after photothrombosis, brain sections were stained with anti-ionized calcium binding adaptor molecule 1 (Iba1), a well-known marker for activated microglia, CD68 for the CD68 antigen indicating phagocytosis, NG2 which is co-expressed on morphologically activated microglia and also recognized on oligodendrocyte and microglial precursors, NeuN to identify surviving neurons, as well as markers of microglial polarization. As pro-inflammatory M1 marker inducible nitric oxide synthase (iNOS) was stained, as anti-inflammatory M2 marker CD206, Ym1 and Arginase 1 (Arg1) were used. To further assess subtle microglial activation we stained for Isolectin B4 and MHC-II/ Ox6. Furthermore, the astrocytic marker glial fibrillary acidic protein (GFAP) was stained to analyze glial scarring and Bromodeoxyuridine (BrdU) to assess proliferation (compare Tab. 1).

antibody	**marked cell population**	**reference**
IbA1 (anti-ionized calcium binding adaptor molecule 1)	activated microglia	Wako, Neuss, Germany; cat# 019-19741
CD68	CD68 antigen indicating phagocytosis	Bio-Rad Laboratories, Hercules, USA; cat# MCA341
NG2	Oligodendrocyte and microglial precursors	Abcam, Cambridge, UK; cat# ab50009-100
NeuN	surviving neurons	Merck Millipore, Massachusetts,

		USA; cat# MAB377
iNOS (inducible nitric oxide synthase)	M1 polarized microglia	Abcam, Cambridge, UK; cat# ab15323
CD206	M2 polarized microglia	R&D Systems, Minneapolis, USA; cat# AF2535
Ym1	M2 polarized microglia	Stemcell Technologies, Vancouver, Canada; cat# 01404
Arg1 (Arginase 1)	M2 polarized microglia	Abcam, Cambridge, UK; cat# ab60176
BrdU (Bromodeoxyuridine)	cell proliferation	clone BU-33, Sigma-Aldrich, Munich, Germany, cat# B-2531
GFAP (glial fibrillary acidic protein)	astrocytes	Merck Millipore, Massachusetts, USA; cat# MAB360
Isolectin GS-B4 (**from Griffonia simplicifolia, Alexa Fluor™ 488 Conjugate**)	microglial activation	Thermo Fisher Scientific, Massachusetts, USA; cat# I21411
MHC-II (Ox6)	microglial activation	AbD Serotec/ Bio-Rad Antibodies, Puchheim, Germany; cat# MCA46R

Table 1: Overview of the antibodies used

Depending on the antibody, the sections were either prepared with 4% PFA or Acetone (100 %, 50 %) for 15 min or 30 min at room temperature (RT), or overnight at 4 °C. Afterwards, the slides were washed in 0.1 M PBS, quenched in H_2O_2 (in 3,3'-diaminobenzidine (DAB)-staining), washed in 0.1 M PBS again and blocked with 5% normal goat serum, 5% normal donkey serum (Jackson Immuno Research Laboratories, Baltimore, USA), or 5% normal horse serum (Vector Laboratories, Burlingame, CA, USA) in 0.1 M PBS (with or without 0.3 % Triton X) for 45 min. The sections were incubated with the primary antibody or antibody conjugate (IB4) overnight at 4 °C.

After rinsing and washing in 0.1 M PBS, the secondary antibodies biotinylated goat anti-rabbit IgG, horse anti-mouse IgG or horse anti-goat IgG (Vector Laboratories, Burlingame, CA, USA) were applied and incubated for 30 min.

For visualization with light microscopy, the ABC Elite Kit (Vector Laboratories, Burlingame,

CA, USA) followed by DAB (Sigma Aldrich, Munich, Germany) as final reaction product.

Secondary antibodies used for fluorescence microscopy were donkey anti-rabbit 488 IgG, donkey anti-goat 568 IgG, donkey anti-mouse 488 IgG, goat anti-mouse 488, goat anti-rabbit 568 (Alexa Fluor, Invitrogen/Life Technologies, Carlsbad, CA, USA), and counterstaining with Hoechst 33342 (Life Technologies, Darmstadt, Germany).

To assess the delineation of the primary infarct region, serial PFA fixed sections with 200 µm intervals were stained with the Toluidine Blue O (TBO; Sigma-Aldrich, Munich, Germany). Before staining, slides were fixed in 4 % PFA for 10 min and consecutively washed in 0.1 M PBS. Slides were then stained in an aqueous solution of 0.05 % TBO for 30 sec and immediately washed in ddH_2O for at least 30 sec afterwards. After dehydration in an ascending alcohol series for at least 30 sec per step, slides were incubated for 1 mi. in Roti Histol (Carl Roth, Karlsruhe, Germany) and covered in DPX Mountant medium (Sigma-Aldrich, Munich, Germany).

2.3. Image Analysis

2.3.1 Histology and immunohistochemistry

Representative images of the ipsi- and contralateral nuclei ventral anterior (VA) resp. ventral lateral (VL) of the thalamus, of the ventral posterolateral (VPL) area and the subventricular zone (SVZ) were taken using an inverted fluorescence phase-contrast microscope (Keyence BZ-9000E, Osaka, Japan) with 4x, 20x and 40x objectives.

To quantify the stainings described above (cf. 2.2), cells per area of the representative images were counted.

Slides stained with TBO were analyzed under a stereo microscope with an overall magnification of 7x for all slides (Zeiss SteREO Lumar V12, Carl Zeiss, Oberkochen, Germany).

2.3.2 Infarct Volume Analysis

The infarct volume was calculated using sequential brain sections (every 200 µm, corresponding to every 10th slide) stained with TBO and analyzed in Axio Vision software (Carl Zeiss, Oberkochen, Germany). Therefore, freehand forms were drawn around the primary lesion. With the internal scale, determined by the images, the chosen area was plotted by the software for each slide. To extrapolate the analyzed area to a total infarct volume, each result was multiplied by 10 and summed up for every brain. The resulting volume was given in mm³. Manual measurements and volume calculations with the formula for a frustum $V=(1/3)h[A1+\sqrt{(A1*A2)}+A2]$ were used to compare and verify the results obtained by the software.

2.3.3 Autoradiography

Autoradiograms were analyzed with the commercial software AIDA Image Analyzer (Raytest Isotopenmessgeräte, Straubenhardt, Germany). To evaluate the tracer uptake, regions of interest (ROIs) in thalamic nuclei and a corresponding reference region in the contralateral hemisphere were set. A constant offset in the software was set to enhance the precision of the ROI size definition and to delineate all D-CIS-[^{18}F]FPRO-positive areas. A circular background ROI was set on an empty space on the plate for background determination. To compare the tracer uptake and taking respect to the variances in weight of the animals and applied tracer amount, standardized uptake values (SUV) of those ROIs were calculated according to the formula: (ROI radioactivity/injected dose)*animal weight. SUV ratios between thalamic ROIs and reference regions were calculated afterwards. Determination of total D-CIS-[^{18}F]FPRO uptake into thalamic nuclei of the brain was calculated by summing up the SUV of each ROI for all D-CIS-[^{18}F]FPRO-positive areas throughout the brain (SUV_{sum}).

For investigation of the [^{3}H]-Thymidine uptake in the SVZ two identical, rectangular ROIs of the same size were laid over ipsi- and contralateral ventricles. Six representative slides of the same area in each brain were chosen and compared between treatment and control groups. Mean SUVs for each animal and SUV ratios between ipsi- and contralateral hemispheres were calculated as above. For this evaluation, a background ROI was set as described before, as well.

2.4 Statistical Analysis

Statistical evaluations were performed using the GraphPad Prism software and Microsoft Excel. First, data sets were tested for normal distribution with the D'Agostino Pearson omnibus normality test for $n \geq 8$ or Shapiro-Wilk normality or Kruskal-Wallis test for $n < 8$. Normally distributed data sets were analyzed with a parametric test (unpaired t-test for two samples, for unequal variances a Welch's t-test was assigned). Non-normal distributed data required a nonparametric test (Mann-Whitney test for two samples). Correlations were analyzed using Pearson correlation analysis. The *p*-value was set at 0.05 for statistical significance. For analysis of ipsi- versus contralateral sides in the same animal, a paired analysis with the above named requirements for distribution was used. Cell counts in histological analyses were expressed as either the absolute numbers, or the difference between ipsilateral and contralateral numbers. Histological analysis included $n = 8$ rats in the OPN group and $n = 7$ in the placebo group. Due to loss of tissue on phosphoimager plates, only six animals from each group could be used for autoradiographic analyses.

3. Results

3.1 Quantification of ischemic lesion after photothrombosis

OPN treatment did not significantly change the infarct volume although it tended to be smaller (p = 0.26; OPN: 22.26 ± 5.326, placebo: 40.23 ± 13.91, Fig. 1a, b, c, d). This trend was reproduced by manual measurement and volume analysis (p = 0.146; data not shown). Generally, infarct size correlated positively with the amount of Iba1-positive cells in the ventral anterior (VA) and ventral lateral (VL) nuclei and in the ventral posterolateral (VPL) nucleus of the thalamus (VPL: p = 0.0129, r^2 = 0.52; Fig. 2g; VA/VL: p < 0.0001, r^2 = 0.98).

3.2 Treatment with OPN decreased in parallel secondary neurodegeneration and microglial activation

Remote from the ischemic focus, ischemia induced Iba1-positive microglia activation (measured as cells per field of view) in the ipsilateral thalamus eight days after cortical infarction. This effect was observed in both the OPN and placebo group (Fig. 2a, c, d, f, g). Comparing OPN and placebo groups, OPN reduced the accumulation of Iba1-positive microglia in the ipsilateral VPL of the thalamus (p = 0.0036; OPN: 33.52 ± 5,304; placebo: 66.07 ± 7.731; Fig. 2a, d). Morphologically, microglia were found in different states of activation. Iba1 staining revealed a spectrum of activated microglia phenotypes with elongated processes and small cell bodies. The closer to the center of the Iba1-positive area in the VPL and the VA/VL nuclei, the more microglia had shorter processes and larger cell bodies (Fig. 2a). In the NeuN-staining for neuronal cell bodies, we observed a significant reduction of neurons in the ipsilateral thalamus of control animals, reflecting neuronal loss (VPL: p = 0.0154; OPN: 2 ± 4.914; VA/VL: p < 0.0001; OPN: 20.22 ± 5.217; placebo: -44.57 ± 9.566; Fig. 2b, e). By contrast, OPN-treated animals had no significant difference between both thalami (data not shown, placebo-treated animals: Iba1 cell count/ area ipsilateral versus contralateral, p = 0.0068, OPN-treated animals: Iba1 cell count/ area ipsilateral versus contralateral, p = 0.792).

Areas of microglia activation matched areas of neuronal loss (Fig. 2c), confirmed by quantitative analysis (Fig 2f). There was a negatively proportional relationship between NeuN+ and Iba1+ cells, with less NeuN+ cells coinciding with more Iba1+ cells (Fig. 2 f). Furthermore, Iba1+ cell counts correlated with the infarct volume ($p = 0.0129$; $r^2 = 0.515$; Fig 2g) as well as with the extent of thalamic degeneration, as revealed by autoradiography ($p < 0.0001$; $r_{Pearson} = 0.93$; Fig. 5e).

In summary, data points of OPN-treated and placebo groups were distinct, suggesting a shift of Iba1+/NeuN+, Iba1+/ infarct volume as well as Iba1+ counts/ D-CIS-[^{18}F]FPRO uptake by OPN treatment (Fig. 2f, g; 5c).

3.3 Activation of phagocytic cells is attenuated by OPN

To further classify microglial activation, we assessed M1/M2 polarization markers such as Arg1 and Ym1 for M2 polarization, and iNOS for M1 polarization, CD68 (ED1) for phagocytosis, CD206 for perivascular macrophages, Ox6 for expression of MHC class II, and Isolectin B4 (IB4) for microglial activation as described by Streit and Kreutzberg (Streit and Kreutzberg 1987). In contrast to earlier findings at the infarct site (Ladwig et al. 2017), the expression of M1/M2 markers was scarce in thalamic areas showing secondary neurodegeneration. Most Iba1+ microglia neither expressed M1 nor M2 markers on a detectable level (data not shown). Constitutively, perivascular microglia expressed CD206. Numbers of CD206-positive cells per area did not significantly change in the VA/VL or the VPL of placebo animals (VA/VL: $p = 0.1$; VPL: $p = 0.65$; Fig. 3a, c). The majority of these cells could be found in a perivascular position and scarcely in the parenchyma (Fig. 3a). CD68-positive phagocytic cells were found significantly elevated in the VPL of placebo-treated animals ($p = 0.035$; OPN: 4.25 ± 2.002; placebo 20.57 ± 7.116; Fig. 3b,d). OPN treatment attenuated the expression of CD68 antigen in VPL (Fig. 3d). IB4 staining revealed a

subpopulation of Iba1+ microglia, which appeared morphologically activated with larger cell bodies and stout processes (Fig. 8b). OPN-treated animals showed a significant decrease in the ipsilateral thalamus compared to controls (p = 0.017; OPN: 16.22 ± 3.779; placebo: 46.10 ± 12.35; Fig.8a). Exemplary stainings of Ox6 showed a selective population of microglia with MHC class II upreagulation, which could only be found in the primary area of photothrombosis and the ipsilateral thalamus. In line with above shown results, OPN-treated animals showed a trend towards a decreased expression of MHC II on microglia (Fig. 8c).

3.4 Increased BINCs in the ipsilateral thalamus in placebo-treated animals

BINCs (*b*rain *I*bA1- and *N*G2-positive *c*ells) have been described as a discrete subpopulation of activated microglia. We stained for NG2 and found two morphologically separate cell-types: firstly the NG2- and Iba1- double positive cells (BINCs), activated microglia with shorter processes and larger cell bodies (stellate cells, Fig. 4a, left row), and secondly a cell-type with a small cell body and two long processes reminiscent of oligodendrocytes that did not co-label with Iba1 (Fig. 4a, right row). BINCs were elevated in the ipsilateral VPL and VA/VL of the placebo group; the increase was attenuated in the OPN-treated group (VPL: p = 0.0093, OPN: 15.38 ± 5.4, placebo: 53.86 ± 16.33; VA/VL: p = 0.04, OPN: 4.5 ± 4.64, placebo: 29.14 ± 10.36; Fig. 4b, c).

3.5 Degeneration in the thalamus revealed by D-CIS-[^{18}F]FPRO autoradiography

Ex vivo, secondary neurodegeneration of the thalamus was assessed using autoradiography. D-CIS-[^{18}F]FPRO accumulated in the area of infarction and the area of degeneration in the ipsilateral thalamus (Fig. 5a, b). Although the D-CIS-[^{18}F]FPRO-positive volume in the thalamus did not differ between groups (not shown), the total amount of uptake in thalamus

(SUV sum) was decreased in OPN-treated versus placebo animals, suggesting OPN to attenuate degeneration ($p = 0.01$; Fig. 5c). As evidence for the assumption that a larger infarct results in more thalamic degeneration, the total amount of D-CIS-[^{18}F]FPRO uptake (SUV sum) highly correlated with the infarct volume ($r_{Pearson} = 0.931$, $p < 0.0001$; Fig. 5d). Corroborating the results from NeuN immunohistochemistry, data points of OPN and placebo animals were separated: with a given infarct volume, OPN-treated animals tended to display less degeneration in the thalamus in comparison to placebo-treated rats as assessed by D-CIS-[^{18}F]FPRO SUV sum (Fig. 5d-f, cp. Fig. 2f-g). In line with these results, NeuN positive cells correlated negatively with D-CIS-[^{18}F]FPRO SUV uptake in the thalamus. At a given level of degeneration (D-CIS-[^{18}F]FPRO SUV sum) OPN-treated animals tended to display less NeuN+ cell loss (Fig. 5f).

3.6 Local microglia proliferation in the thalamus

Local proliferation is another hallmark of microglial activation that was addressed by intravital BrdU injections. Most prominently, the ipsilateral thalamus of placebo-treated animals displayed numerous double Iba1+ and BrdU+ cells, defining a proliferating microglia subpopulation (Fig. 6a). Iba1+ and BrdU+ cells were significantly reduced in the VPL of OPN-treated animals compared to placebo, but absolute numbers were small ($p = 0.0056$, OPN: 5 ± 1.4, placebo: 14.5 ± 2.56; Fig. 6b). In line with the scarcity of proliferating cells in the thalamus, autoradiography with [^{3}H]thymidine failed to display any discernable spot in the thalamic area (not shown). Instead, [^{3}H]thymidine autoradiography showed tracer accumulation in the infarct area as well as in the SVZ as a major niche of neural stem cells (Fig 6c, d).

Proliferation was increased in the SVZ ipsilateral to the OPN/placebo injection in placebo-treated animals as assessed by [^{3}H]thymidine ($p = 0.007$; paired analysis, mean of differences 0.01033, $R^2 = 0.7381$, pairing: r = 0.9987); Fig. 6e), while this asymmetry was attenuated in

OPN-treated animals (Fig. 6e,). Consequently, the ipsilateral/ contralateral ratio showed a decease in OPN-treated animals ($p = 0.016$; OPN: 1.082 ± 0.02472, placebo: 1.211 ± 0.04577).

3.7 Astrogliosis in the area of secondary neurodegeneration is attenuated in OPN-treated animals

As with microglia, astrocytes serve as microsensors of underlying neuronal damage corresponding to the degree of the lesion. We evaluated numbers of GFAP+ astrocytes and observed a quantitative decrease in intensity of staining as well as a significant decrease in numbers in OPN-treated animals compared to controls in the VPL and VA/VL of the ipsilateral thalamus (VPL: $p = 0.0019$, OPN: 16.19 ± 4.721, placebo: 44.86 ± 5.749; VA/VL: $p = 0.0343$, OPN: 16.06 ± 4.480, placebo: 56.93 ± 14.96; Fig. 7).

4. Discussion

In this study, we investigated the effect of intracerebroventricular administration of OPN on secondary neurodegeneration resulting from cortical ischemic stroke in thalamic nuclei in rats. OPN attenuated neurodegeneration and modulated microglia activation. Whereas typical markers of M1 and M2 polarization were absent, distinct subpopulations were affected, namely BINCs and phagocytosing CD68+ microglia. The radiotracers D-CIS-[^{18}F]FPRO and [^{3}H]thymidine detected neurodegeneration and cell proliferation, respectively.

Secondary neurodegeneration is a well-described phenomenon in stroke (Iizuka et al. 1990; Myers et al. 1991; Schroeter et al. 1999; Pappata et al. 2000). It is assumed that this process occurs in a corticotropic fashion alongside reciprocal thalamo-cortical circuits (Myers et al. 1991; Schroeter et al. 1999). The attenuation of secondary neurodegeneration and inflammation in the thalamus has been shown to reduce the functional deficit after a stroke

(Schroeter et al. 2006; Villa et al. 2007). Overall, we found a substantially decreased inflammatory reaction, as well as neurodegeneration in the ipsilateral thalamus in OPN-treated animals, while the infarct volume was not significantly reduced. This finding is in line with earlier data on OPN knockout mice, suggesting an unaltered infarct development while secondary neurodegeneration, inflammatory gene expression, microglial activation, and neuronal degeneration were enhanced by OPN knockdown (Schroeter et al. 2006). Studies that showed a significant reduction in infarct volume used shorter time periods after infarction (48h, 96h) as opposed to 8 days post infarction in our experiment and different stroke models (Meller et al. 2005; Doyle et al. 2008). One study showed a significantly reduced infarct volume after 24h, however, no effect on brain atrophy after 7 weeks (Chen et al. 2011). Photothrombosis is a cortical model of permanent ischemia without reperfusion and, importantly, little 'tissue at risk'. By contrast, transient MCAo, a model with reperfusion and extensive tissue at risk, revealed effects of multiple pharmacological agents on infarct volume, which, however, to date failed to be reproduced in permanent ischemia models or, even more relevant, in an attempt to overcome the translational roadblock.

Iba1 is a well-established microglia marker to readily detect activated microglia in CNS parenchyma. Microglial activation is very sensitive to any tissue damage in a highly regulated fashion (Orihuela et al. 2016). The extent of activation parallels the extent of neuronal damage. We observed that a single intracerebroventricular injection of OPN potently attenuated both neuronal damage and microglial activation (cf. Fig. 2). Even more, OPN shifted the ratio of Iba1 versus NeuN: for a given level of neuronal damage, OPN attenuated the microglial responses (cf. Fig. 2f), suggesting a primary and direct effect of OPN on microglia, in line with previous findings in knockout mice and in the infarct tissue (Schroeter et al. 2006; Rabenstein et al. 2016; Ladwig et al. 2017). Further we hypothesize from those findings that attenuation of microglial activation in turn leads to neuroprotection. Corroborating the histological results,

autoradiographical data confirmed this correlation and the influence of OPN on the inflammation versus neuronal survival ratio (Fig. 2 f, g; 5 c).

To date, little is known about M1/M2 microglial polarization states in secondary neurodegeneration. Interestingly, although we saw densely packed Iba1-positive morphologically activated microglia, IB4- and Ox6-positive microglia confirming the presence of an activated and in the latter case even pro-inflammatory phenotype (cf. Fig.8) and some CD68-positive cells suggesting phagocytic activity, we could not detect M1 or M2-markers such as Arg1, iNOS or Ym1, all of them found in abundance in the primary site of the ischemic injury (constituting a positive control on the same section) (Perego et al. 2011; Hu et al. 2012; Ladwig et al. 2017). As Ox6/MCH II is a marker found upregulated mostly on classically activated microglia (Chávez-Galán et al. 2015), it was surprising to find an upregulation in MHC II but not in iNOS. This lack of effect might be due to the generally milder and more chronic nature of inflammation in remote areas. To this end, we hypothesize that the M1 and M2 paradigm does not describe discrete activation states. Instead, we suggest in line with our *in vitro* results that M1 and M2 activation of microglia constitute a dynamic and a more gradual process (Vay et al. 2018) ,coined the“ color wheel of macrophages” in the peripheral monocyte/macrophage system (Mosser and Edwards 2008).

Apart from microglia, oligodendrocytes are predominantly inflicted in the regeneration of several CNS diseases. Remyelination is a primary therapeutic target for treatment of multiple sclerosis or spinal cord injury (Bhatt et al. 2014; Chamberlain et al. 2016). After stroke, precursors get recruited, mature to myelinating oligodendrocytes, and help to restore damaged white matter (Itoh et al. 2015). We used NG2 as a marker for oligodendrocyte precursor cells (OCPs) to identify the regenerative potential. Interestingly, we found two types of NG2

positive cells. First, a population morphologically similar to OCPs with two long processes and a small soma (cf. Fig 4, “non-BINCs”), and second, a population immunohistochemically co-expressing Iba1 and morphologically identified as activated microglia (BINCs). BINCs (*b*rain *I*bA1- and *N*G2-positive *c*ells) are highly proliferative cells with phagocytic properties predominantly found in the core of a large cerebral infarction in rats (Matsumoto et al. 2008; Smirkin et al. 2010). Detection of BINCs starts three days after stroke in the ischemic core with a peak at day 7. It has been postulated, that BINCs neither derive from resting microglia nor NG2-positive cells (non-BINCs) and have been shown to exert protective effects on the lesion core of an experimental stroke (Matsumoto et al. 2008). Our results show a decrease in BINCs in the ipsilateral thalamus in OPN-treated animals concomitant with a decrease in inflammation.

Similar to microglia, astrocytes function as microsensors of inflammation and have putative function in regulating inflammatory reaction of microglia/ macrophages after stroke (Becerra-Calixto and Cardona-Gómez 2017). In our previous work we described a polarization of astrocyte processes towards the infarct area in the margin after application of OPN (Ladwig et al. 2017), which was in line with results from an OPN knockout model (Gliem et al. 2015). Other studies have shown a direct effect of OPN-KO on downregulation of GFAP on astrocytes (Ikeshima-Kataoka et al. 2018). Interestingly, in the thalamus we found an increase in staining and in numbers of GFAP+ astrocytes in the ipsilateral thalamus after stroke compared to contralateral (Fig. 7). This increase could be partially attenuated by OPN application. In contrast to previous studies, our results show a downregulation of GFAP+ cells after OPN, which might be due less to direct effects of OPN on astrocytes and rather ascribed to the attenuation of inflammation in general prompting less astrocytic reaction.

Previous studies have found resident microglia locally proliferating after focal cerebral ischemia while infiltrating macrophages were not positive for BrdU (Denes et al. 2007). As postulated by Denes et al., proliferation hallmarks a more sustained microglial activation. In line with the other results, OPN treatment reduced the number of proliferating microglia. The notion of proliferating microglia makes it even more remarkable that microglia activation lacked any M1/M2 markers at the same time.

With these results in mind, we were looking for a method that allows visualizing these OPN effects *in vivo*. Autoradiography allowed us to screen PET tracers with high spatial resolution and reasonable effort *ex vivo*. The tracer D-CIS-[^{18}F]FPRO is a sensitive marker for secondary neurodegeneration after stroke (Langen et al. 2007). Moreover, this tracer can be used for positron emission tomography (PET) imaging technique in both animal and human studies (Langen et al. 2007; Geisler et al. 2013). It, therefore, offers a translational perspective, i.e., to visualize secondary thalamic neurodegeneration *in vivo*. We were able to confirm our immunohistochemical results, i.e., we observed an attenuation of D-CIS-[^{18}F]FPRO uptake in the ipsilateral thalamus in OPN-treated animals, corroborating the immunohistochemical results of reduced neuronal damage and degeneration. Beyond postischemic secondary neurodegeneration, our findings extend the feasibility of D-CIS-[^{18}F]FPRO to paradigms of antero- or retrograde, and transneuronal degeneration as well as slowly evolving neuronal loss.

[^{3}H]thymidine is a well-known tracer for autoradiography to visualize proliferating cells. Using the PET tracer [^{18}F]FLT (3'-deoxy-3'-[^{18}F]fluoro-L-thymidine), corresponding data can be obtained *in vivo* (Rueger et al. 2010). In recent studies, [^{18}F]FLT-PET has mirrored the effects of pharmacological interventions on neural stem cells (Rueger et al. 2012; Klein et al. 2014, 2016; Hucklenbroich et al. 2014). However, we failed to detect [^{3}H]thymidine uptake in the

thalamus in this study, possibly due to minute amounts of proliferating microglia. By chance, we detected a higher uptake of [^{3}H]thymidine in the ipsilateral vs. contralateral SVZ in placebo animals. This result is in line with earlier findings of OPN to increase survival and proliferation in neural stem cells in culture (Rabenstein et al. 2015) as well as *in vivo* (Rogall et al. 2018). Hence, we have gathered evidence that OPN effects are pleiotropic, multi-facetted, and multi-targeting: they address microglia, neurons, and neural stem cells in distinct ways. Having in mind that microglia is the main cellular endogenous source of OPN after stroke (Ellison et al. 1998), our study adds substantial evidence to the notion that OPN is a main candidate to govern cell-cell interactions between microglia, neurons, and stem cells in tissue damage and repair, highlighting microglia as the main target. The time it takes for infarct tissue to trigger the endogenous expression of OPN and thereby stimulate a cascade of inflammatory reactions, can possibly be shortened by exogenous OPN application. This possibly accelerates the process and steers it towards a more protective neuroinflammation with less neurodegenration. This makes it a promising agent for clinical use. A more viable mode of application for human use instead of i.c.v.-injection could be intranasal application, as suggested by Doyle and colleagues, which has been shown to have similarly neuroprotective effects (Doyle et al. 2008). Future studies will have to target the pathways of those interactions as well as dose-response relationships.

Figure Legends

Fig. 1 Infarct volume is not significantly reduced after OPN treatment. (a) Schematic of secondary neurodegeneration in a coronary section of a rat brain displaying the extent and localization of photothrombosis and the interconnected nuclei of the thalamus (VA: ventral anterior; VL: ventral lateral; VPL: ventral posterolateral thalamic nuclei) succumbing to secondary degeneration. (b) Quantification of infarct volume in OPN-treated animals compared to healthy controls revealed no significant difference between placebo and treatment group. Staggered coronary sections of brains of an OPN-treated (c) and a placebo-treated animal (d) displaying infarcts of similar extent and localization.

Scale bar is 2 mm in c, d. Plot displays individual animal values (dots), mean (bar) and s.e.m (whisker).

Fig. 2 Microglial activation in the thalamus is attenuated and neurodegeneration is reduced in OPN-treated animals (a) Iba1-positive (activated) microglia in the ipsilateral thalamus are reduced in OPN-treated animals. Close-ups show differences in morphological signs of activation: the stoutness of processes, the thickness of cells bodies, and the intensity of staining. (b) NeuN-positive neurons are depleted in the ipsilateral thalamus of control animals. Close-ups show fragmented perikarya in placebo condition and intact neuronal perikarya in the treatment group. (c) Double immunofluorescence of Iba1 (red), and NeuN (green) in exemplary placebo-treated animal. Left picture shows neurons in close proximity to activated microglia (arrows). Areas of pronounced inflammation are depleted of neurons (middle), areas with intact neurons contain less inflammatory cells (right). (d) Quantification of Iba1 in thalamus by area (VPL and VA/VL). Iba1-positive cells are significantly decreased in VPL of the ipsilateral thalamus in OPN-treated animals compared to controls. VA/VL shows a trend. (e) Quantification of NeuN in thalamus by area (VPL and VA/VL). NeuN positive

cells are preserved in VPL and VA/VL of the ipsilateral thalamus in OPN-treated animals compared to controls. (f) Correlation of Iba1 and NeuN staining in VPL. Each dot represents an OPN or placebo-treated animal (green circles vs. red squares). Negative proportional relationship between NeuN- and Iba1-count. (g) Correlation of infarct volume and microglia activation. The larger the infarct, the more microglia activation occurred. With a given infarct volume, OPN-treated animals had less microglia activation; groups did not overlap.

Scale bars are 100 µm in a and b (large pictures), 20 µm in close-ups in a and b, and in c. Bar graphs represent mean ± s.e.m. *** $p < 0.001$, ** $p < 0.001$, *$p < 0.5$. VA: ventral anterior; VL: ventral lateral; VPL: ventral posterolateral thalamic nuclei

Fig. 3 Activation of phagocytic cells is attenuated by OPN (a) CD206-+ cells were found in perivascular (arrow) and parenchymal position (arrowhead). Quantification did not reveal significant differences between groups (c). (b) CD68-staining (CD68/ ED1) for phagocytosing microglia in the thalamus. (d) Quantification revealed upregulation in ipsilateral VPL (placebo group) and attenuation in the OPN group.

Scale bars are 100 µm in a and b. Bar graphs represent mean ± s.e.m. *$p < 0.05$. VA: ventral anterior; VL: ventral lateral; VPL: ventral posterolateral thalamic nuclei

Fig. 4 Less Brain Iba1 NG2 cells (BINCs) are found in the ipsilateral VPL of the thalamus in OPN-treated animals (a) Double immunofluorescence staining of Iba1 and NG2 showing two distinct NG2+ cell populations: BINCs – cells positive for Iba1 as well, and non-BINCs. Exemplary pictures were taken from a placebo-treated animal (left side: ipsilateral VPL, right side: contralateral VPL). (b) Morphology of NG2+ cells in the thalamus in DAB-staining: in control animals, NG2+ cells were predominantly compatible with stellate microglia corresponding to BINC subpopulation of microglia. By contrast, in OPN-treated animals NG2+

cells were small, of comma-like shape suggesting oligodendrocyte precursors. (c) BINCs are quantified in VPL and VA/VL of ipsilateral and contralateral thalamus. BINC numbers decreased in both ipsilateral areas of thalami in OPN-treated animals.

Scale bars are 100 µm in a and b, and 20 µm in close-ups. Bar graphs represent mean ± s.e.m. ** $p < 0.01$. VA: ventral anterior; VL: ventral lateral; VPL: ventral posterolateral thalamic nuclei

Fig. 5 D-CIS-[^{18}F]FPRO uptake visualizes OPN effects on degeneration (a,b) Areas of D-CIS-[^{18}F]FPRO uptake resembles infarct area and ipsilateral thalamus of OPN (a), and placebo-treated animals (b). (c) Quantification of total tracer uptake as SUV sum reveals reduced thalamic D-CIS-[^{18}F]FPRO uptake in OPN-treated animals ($p = 0.01$). (d) SUV sum correlated closely with the infarct volume. With a given infarct volume SUV sum tended to be lower in OPN-treated rats. (e) Correlation of the extent of thalamic degeneration as captured by D-CIS-[^{18}F]FPRO uptake with microglia activation. The more thalamus degenerated, the more microglial activation occurred. With a given thalamic degeneration, microglia activation was attenuated in the OPN-treated group. (f) Correlation of D-CIS-[^{18}F]FPRO uptake with neuronal survival. The more degeneration in the thalamus, the less surviving neurons were found. With a given extent of thalamic degeneration neuronal survival was ameliorated in the OPN-treated group.

Bar graphs represent mean ± s.e.m. *** $p < 0.001$, * $p < 0.05$.

Fig. 6 Proliferative activity in the thalamus and subventricular zone. (a) Immunofluorescence co-staining of Iba1 and BrdU shows increased proliferation in the ipsilateral thalamus of placebo-treated animals. (b) Quantification of ipsilateral thalamic

microglial proliferation. Proliferating microglia in ipsilateral thalamus are overall low in number and significantly decreased in the VPL of the OPN-treated group. (c, d) Exemplary [^{3}H]thymidine autoradiographic sections, tracer accumulation in the infarct and the subventricular zones (SVZ) can be discerned. (e) Box and whisker plot of tracer uptake in SVZ. In placebo animals uptake tended to be lower, and there was a small but significant difference in ipsilateral compared to contralateral SVZ. (f) Regarding the SUV ratio of ipsi- to contralateral uptake in the SVZ, data show a significant difference between OPN-treated and placebo-treated rats.

Scale bar is 100 µm and 20 µm in close-ups in a. Bar graphs represent mean ± s.e.m. * $p <$ 0.05,** $p < 0{,}01$. VA: ventral anterior; VL: ventral lateral; VPL: ventral posterolateral thalamic nuclei

Fig. 7 Astrocytosis in ipsilateral thalamus after after photothrombosis is attenuated by OPN. (a) GFAP - positive cells are reduced in the ipsilateral thalamus in OPN versus placebo-treated animals (b) Quantification of GFAP in thalamus by area (VPL and VA/VL). GFAP - positive cells are significantly decreased in VPL and VA/VL of the ipsilateral thalamus in OPN-treated animals compared to controls.

Scale bar is 100 µm in a. Bar graphs represent mean ± s.e.m. * $p < 0.05$,** $p < 0{,}01$, VA: ventral anterior; VL: ventral lateral; VPL: ventral posterolateral thalamic nuclei.

Fig. 8 Markers of microglial activation are attenuated by OPN treatment. (a) Isolectin B4 (IB4) and Iba1 double-immunofluorescence staining show attenuated microglial activation in the ipsilateral thalamus of OPN-treated animals. (b) Magnified images of IB4/Iba1 staining showing several double positive cells (white arrow heads) in an exemplary placebo-treated animal compared to an OPN-treated animal with sparse overlap. (c) Double

immunofluorescence staining of MHC class II/ Ox6 and Iba1 delineating a distinct population of microglia with upregulated MHC II receptors in the ipsilateral thalamus after stroke. Quantification showed a trend towards decreased upregulation in OPN-treated animals. White arrow heads indicate double labeled cells.

Scale bar is 100 µm in a, b and close ups in c (lower row) and 500 µm in 4x pictures of entire thalamus in c (upper row). Bar graphs represent mean ± s.e.m. * $p < 0.05$.

Ethical approval: All applicable international, national, and/or institutional guidelines for the care and use of animals were followed. All procedures performed in the studies involving animals were in accordance with the ethical standards of the institution at which the studies were conducted.

References

Becerra-Calixto A, Cardona-Gómez GP (2017) The Role of Astrocytes in Neuroprotection after Brain Stroke: Potential in Cell Therapy. Front Mol Neurosci 10:. doi: 10.3389/fnmol.2017.00088

Bhatt A, Fan L-W, Pang Y (2014) Strategies for myelin regeneration: lessons learned from development. Neural Regen Res 9:1347–1350. doi: 10.4103/1673-5374.137586

Butler WT (1989) The nature and significance of osteopontin. Connect Tissue Res 23:123–136

Butler WT (1995) Structural and functional domains of osteopontin. Ann N Y Acad Sci 760:6–11

Chamberlain KA, Nanescu SE, Psachoulia K, Huang JK (2016) Oligodendrocyte regeneration: Its significance in myelin replacement and neuroprotection in multiple sclerosis. Neuropharmacology 110:633–643. doi: 10.1016/j.neuropharm.2015.10.010

Chen W, Ma Q, Suzuki H, et al (2011) Osteopontin reduced hypoxia-ischemia neonatal brain injury by suppression of apoptosis in a rat pup model. Stroke J Cereb Circ 42:764–769. doi: 10.1161/STROKEAHA.110.599118

De Vloo P, Morlion B, van Loon J, Nuttin B (2017) Animal models for central poststroke pain: a critical comprehensive review. Pain 158:17–29. doi: 10.1097/j.pain.0000000000000722

Denes A, Vidyasagar R, Feng J, et al (2007) Proliferating resident microglia after focal cerebral ischaemia in mice. J Cereb Blood Flow Metab 27:1941–1953. doi: 10.1038/sj.jcbfm.9600495

Denhardt DT, Noda M, O'Regan AW, et al (2001) Osteopontin as a means to cope with environmental insults: regulation of inflammation, tissue remodeling, and cell survival. J Clin Invest 107:1055–1061

Doyle KP, Yang T, Lessov NS, et al (2008) Nasal administration of osteopontin peptide mimetics confers neuroprotection in stroke. J Cereb Blood Flow Metab Off J Int Soc Cereb Blood Flow Metab 28:1235–1248. doi: 10.1038/jcbfm.2008.17

Ellison JA, Velier JJ, Spera P, et al (1998) Osteopontin and its integrin receptor alpha(v)beta3 are upregulated during formation of the glial scar after focal stroke. Stroke J Cereb Circ 29:1698–1706; discussion 1707

Freret T, Chazalviel L, Roussel S, et al (2006) Long-term functional outcome following transient middle cerebral artery occlusion in the rat: correlation between brain damage and behavioral impairment. Behav Neurosci 120:1285–1298. doi: 10.1037/0735-7044.120.6.1285

Fu G-X, Xu C-C, Zhong Y, et al (2012) Aldosterone-induced osteopontin expression in vascular smooth muscle cells involves MR, ERK, and p38 MAPK. Endocrine 42:676–683. doi: 10.1007/s12020-012-9675-2

Geisler S, Willuweit A, Schroeter M, et al (2013) Detection of remote neuronal reactions in the Thalamus and Hippocampus induced by rat glioma using the PET tracer cis-4-[18F]fluoro-□-proline. J Cereb Blood Flow Metab 33:724–731. doi: 10.1038/jcbfm.2013.8

Giachelli CM, Liaw L, Murry CE, et al (1995) Osteopontin expression in cardiovascular diseases. Ann N Y Acad Sci 760:109–126

Gliem M, Krammes K, Liaw L, et al (2015) Macrophage-derived osteopontin induces reactive astrocyte polarization and promotes re-establishment of the blood brain barrier after ischemic stroke. Glia. doi: 10.1002/glia.22885

Hedtjärn M, Mallard C, Hagberg H (2004) Inflammatory gene profiling in the developing mouse brain after hypoxia-ischemia. J Cereb Blood Flow Metab Off J Int Soc Cereb Blood Flow Metab 24:1333–1351. doi: 10.1097/01.WCB.0000141559.17620.36

Hu X, Li P, Guo Y, et al (2012) Microglia/macrophage polarization dynamics reveal novel mechanism of injury expansion after focal cerebral ischemia. Stroke J Cereb Circ 43:3063–3070. doi: 10.1161/STROKEAHA.112.659656

Hucklenbroich J, Klein R, Neumaier B, et al (2014) Aromatic-turmerone induces neural stem cell proliferation in vitro and in vivo. Stem Cell Res Ther 5:100. doi: 10.1186/scrt500

Hur EM, Youssef S, Haws ME, et al (2007) Osteopontin-induced relapse and progression of autoimmune brain disease through enhanced survival of activated T cells. Nat Immunol 8:74–83. doi: 10.1038/ni1415

Iizuka H, Sakatani K, Young W (1990) Neural damage in the rat thalamus after cortical infarcts. Stroke 21:790–794

Ikeshima-Kataoka H, Matsui Y, Uede T (2018) Osteopontin is indispensable for activation of astrocytes in injured mouse brain and primary culture. Neurol Res 40:1071–1079. doi: 10.1080/01616412.2018.1517995

Itoh K, Maki T, Lok J, Arai K (2015) Mechanisms of cell-cell interaction in oligodendrogenesis and remyelination after stroke. Brain Res 1623:135–149. doi: 10.1016/j.brainres.2015.04.039

Kato A, Okura T, Hamada C, et al (2014) Cell stress induces upregulation of osteopontin via the ERK pathway in type II alveolar epithelial cells. PloS One 9:e100106. doi: 10.1371/journal.pone.0100106

Klein R, Blaschke S, Neumaier B, et al (2014) The synthetic NCAM mimetic peptide FGL mobilizes neural stem cells in vitro and in vivo. Stem Cell Rev 10:539–547. doi: 10.1007/s12015-014-9512-5

Klein R, Mahlberg N, Ohren M, et al (2016) The Neural Cell Adhesion Molecule-Derived (NCAM)-Peptide FG Loop (FGL) Mobilizes Endogenous Neural Stem Cells and Promotes Endogenous Regenerative Capacity after Stroke. J Neuroimmune Pharmacol Off J Soc NeuroImmune Pharmacol 11:708–720. doi: 10.1007/s11481-016-9694-5

Kumar S, Sharma P, Kumar D, et al (2013) Functional characterization of stromal osteopontin in melanoma progression and metastasis. PloS One 8:e69116. doi: 10.1371/journal.pone.0069116

Ladwig A, Walter HL, Hucklenbroich J, et al (2017) Osteopontin Augments M2 Microglia Response and Separates M1- and M2-Polarized Microglial Activation in Permanent Focal Cerebral Ischemia. Mediators Inflamm 2017:. doi: 10.1155/2017/7189421
Langen K-J, Salber D, Hamacher K, et al (2007) Detection of secondary thalamic degeneration after cortical infarction using cis-4-18F-fluoro-D-proline. J Nucl Med Off Publ Soc Nucl Med 48:1482–1491. doi: 10.2967/jnumed.107.041699

Lee MY, Shin SL, Choi YS, et al (1999) Transient upregulation of osteopontin mRNA in hippocampus and striatum following global forebrain ischemia in rats. Neurosci Lett 271:81–84

Matsumoto H, Kumon Y, Watanabe H, et al (2008) Accumulation of macrophage-like cells expressing NG2 proteoglycan and Iba1 in ischemic core of rat brain after transient middle cerebral artery occlusion. J Cereb Blood Flow Metab Off J Int Soc Cereb Blood Flow Metab 28:149–163. doi: 10.1038/sj.jcbfm.9600519

McKee MD, Nanci A (1996) Secretion of Osteopontin by macrophages and its accumulation at tissue surfaces during wound healing in mineralized tissues: a potential requirement for macrophage adhesion and phagocytosis. Anat Rec 245:394–409. doi: 10.1002/(SICI)1097-0185(199606)245:2<394::AID-AR19>3.0.CO;2-K

Meller R, Stevens SL, Minami M, et al (2005) Neuroprotection by osteopontin in stroke. J Cereb Blood Flow Metab Off J Int Soc Cereb Blood Flow Metab 25:217–225. doi: 10.1038/sj.jcbfm.9600022

Morales-Ibanez O, Domínguez M, Ki SH, et al (2013) Human and experimental evidence supporting a role for osteopontin in alcoholic hepatitis. Hepatol Baltim Md 58:1742–1756. doi: 10.1002/hep.26521

Mosser DM, Edwards JP (2008) Exploring the full spectrum of macrophage activation. Nat Rev Immunol 8:958–969. doi: 10.1038/nri2448

Myers R, Manjil LG, Cullen BM, et al (1991) Macrophage and astrocyte populations in relation to [3H]PK 11195 binding in rat cerebral cortex following a local ischaemic lesion. J Cereb Blood Flow Metab Off J Int Soc Cereb Blood Flow Metab 11:314–322. doi: 10.1038/jcbfm.1991.64

Myles T, Leung LLK (2008) Thrombin hydrolysis of human osteopontin is dependent on thrombin anion-binding exosites. J Biol Chem 283:17789–17796. doi: 10.1074/jbc.M708629200

Ogawa T, Yoshida Y, Okudera T, et al (1997) Secondary thalamic degeneration after cerebral infarction in the middle cerebral artery distribution: evaluation with MR imaging. Radiology 204:255–262. doi: 10.1148/radiology.204.1.9205256

Orihuela R, McPherson CA, Harry GJ (2016) Microglial M1/M2 polarization and metabolic states. Br J Pharmacol 173:649–665. doi: 10.1111/bph.13139

Pappata S, Levasseur M, Gunn RN, et al (2000) Thalamic microglial activation in ischemic stroke detected in vivo by PET and [11C]PK1195. Neurology 55:1052–1054

Perego C, Fumagalli S, Simoni M-GD (2011) Temporal pattern of expression and colocalization of microglia/macrophage phenotype markers following brain ischemic injury in mice. J Neuroinflammation 8:174. doi: 10.1186/1742-2094-8-174

Rabenstein M, Hucklenbroich J, Willuweit A, et al (2015) Osteopontin mediates survival, proliferation and migration of neural stem cells through the chemokine receptor CXCR4. Stemcell Res Ther under revision:

Rabenstein M, Vay SU, Flitsch LJ, et al (2016) Osteopontin directly modulates cytokine expression of primary microglia and increases their survival. J Neuroimmunol 299:130–138. doi: 10.1016/j.jneuroim.2016.09.009

Rogall R, Rabenstein M, Vay S, et al (2018) Bioluminescence imaging visualizes osteopontin-induced neurogenesis and neuroblast migration in the mouse brain after stroke. Stem Cell Res Ther 9:182. doi: 10.1186/s13287-018-0927-9

Rueger MA, Backes H, Walberer M, et al (2010) Noninvasive imaging of endogenous neural stem cell mobilization in vivo using positron emission tomography. J Neurosci Off J Soc Neurosci 30:6454–6460. doi: 10.1523/JNEUROSCI.6092-09.2010

Rueger MA, Muesken S, Walberer M, et al (2012) Effects of minocycline on endogenous neural stem cells after experimental stroke. Neuroscience 215:174–183. doi: 10.1016/j.neuroscience.2012.04.036

Schroeter M, Jander S, Witte OW, Stoll G (1999) Heterogeneity of the microglial response in photochemically induced focal ischemia of the rat cerebral cortex. Neuroscience 89:1367–1377

Schroeter M, Zickler P, Denhardt DT, et al (2006) Increased thalamic neurodegeneration following ischaemic cortical stroke in osteopontin-deficient mice. Brain J Neurol 129:1426–1437. doi: 10.1093/brain/awl094

Smirkin A, Matsumoto H, Takahashi H, et al (2010) Iba1(+)/NG2(+) macrophage-like cells expressing a variety of neuroprotective factors ameliorate ischemic damage of the brain. J Cereb Blood Flow Metab Off J Int Soc Cereb Blood Flow Metab 30:603–615. doi: 10.1038/jcbfm.2009.233

Stoll G, Jander S, Schroeter M (1998) Inflammation and glial responses in ischemic brain lesions. Prog Neurobiol 56:149–171

Streit WJ, Kreutzberg GW (1987) Lectin binding by resting and reactive microglia. J Neurocytol 16:249–260

Vay SU, Flitsch LJ, Rabenstein M, et al (2018) The plasticity of primary microglia and their multifaceted effects on endogenous neural stem cells in vitro and in vivo. J Neuroinflammation 15:226. doi: 10.1186/s12974-018-1261-y

Villa P, van Beek J, Larsen AK, et al (2007) Reduced functional deficits, neuroinflammation, and secondary tissue damage after treatment of stroke by nonerythropoietic erythropoietin derivatives. J Cereb Blood Flow Metab Off J Int Soc Cereb Blood Flow Metab 27:552–563. doi: 10.1038/sj.jcbfm.9600370

Walberer M, Rueger MA, Simard M-L, et al (2010) Dynamics of neuroinflammation in the macrosphere model of arterio-arterial embolic focal ischemia: an approximation to human stroke patterns. Exp Transl Stroke Med 2:22. doi: 10.1186/2040-7378-2-22

Wang KX, Denhardt DT (2008) Osteopontin: role in immune regulation and stress responses. Cytokine Growth Factor Rev 19:333–345. doi: 10.1016/j.cytogfr.2008.08.001

Wang X, Louden C, Yue TL, et al (1998) Delayed expression of osteopontin after focal stroke in the rat. J Neurosci Off J Soc Neurosci 18:2075–2083

Xia C-Y, Zhang S, Gao Y, et al (2015) Selective modulation of microglia polarization to M2 phenotype for stroke treatment. Int Immunopharmacol 25:377–382. doi: 10.1016/j.intimp.2015.02.019

Xiong X-Y, Liu L, Yang Q-W (2016) Functions and mechanisms of microglia/macrophages in neuroinflammation and neurogenesis after stroke. Prog Neurobiol 142:23–44. doi: 10.1016/j.pneurobio.2016.05.001

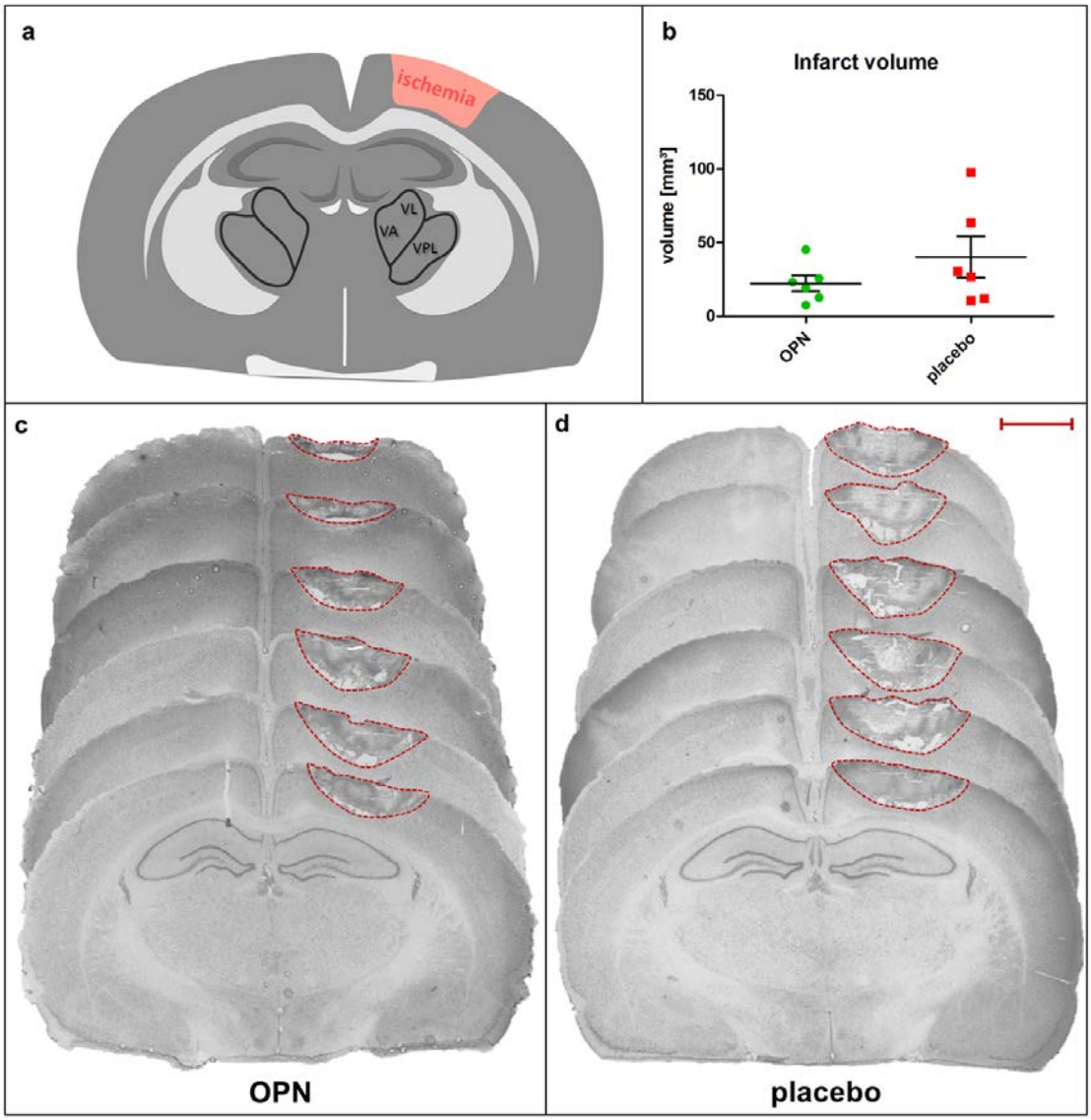
a
ischemia
VL
VA
VPL
b
Infarct volume
volume [mm³]
150
100
50
0
OPN
placebo
c
OPN
d
placebo

Fig.1

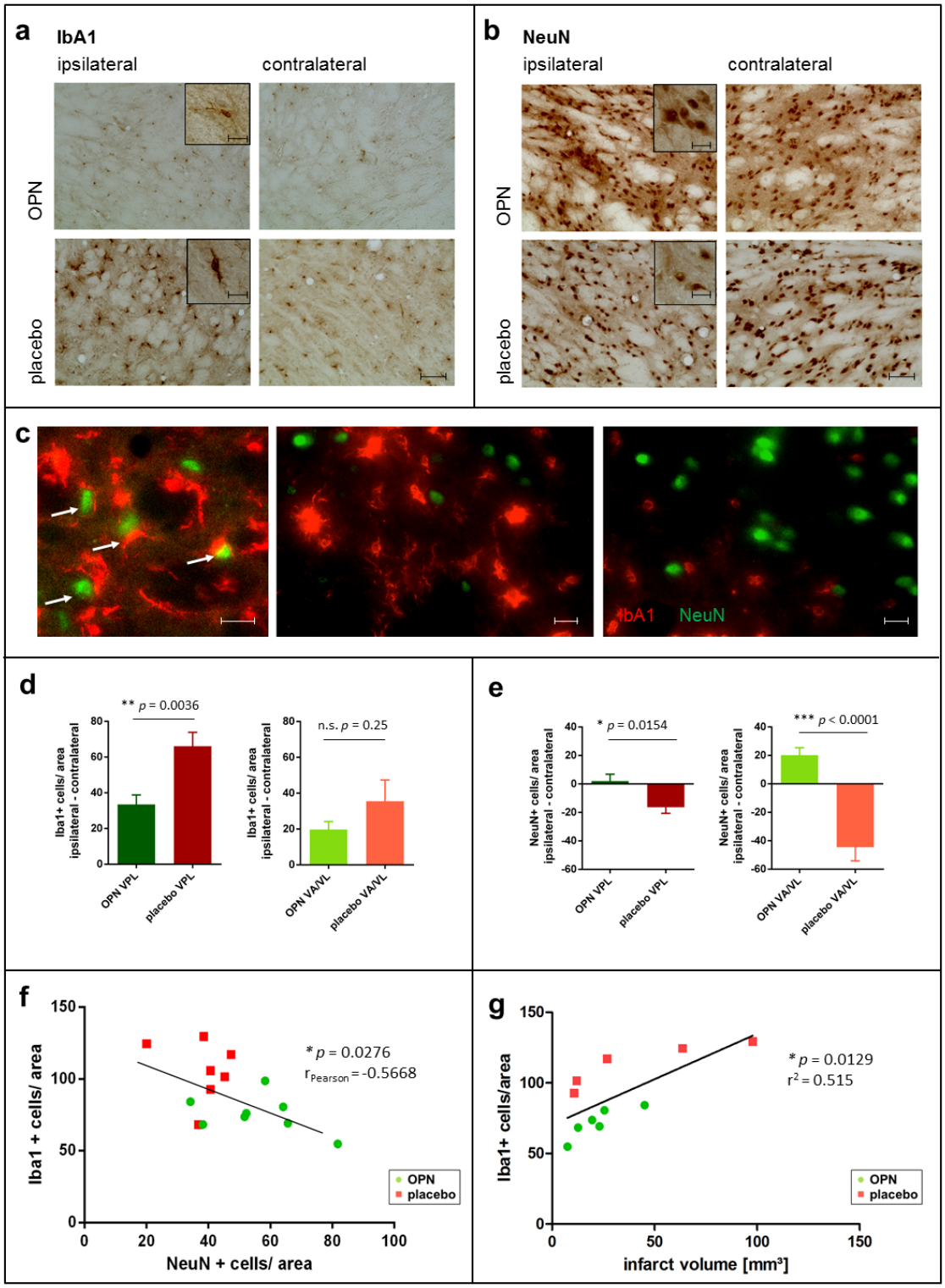
a
IbA1
ipsilateral
contralateral
OPN
placebo
b
NeuN
ipsilateral
contralateral
OPN
placebo
c
IbA1
NeuN
d
** p = 0.0036
n.s. p = 0.25
Iba1+ cells/ area ipsilateral - contralateral
OPN VPL
placebo VPL
OPN VA/VL
placebo VA/VL
e
* p = 0.0154
*** p < 0.0001
NeuN+ cells/ area ipsilateral - contralateral
OPN VPL
placebo VPL
OPN VA/VL
placebo VA/VL
f
* p = 0.0276
r Pearson = -0.5668
Iba1 + cells/ area
NeuN + cells/ area
OPN
placebo
g
* p = 0.0129
r² = 0.515
Iba1+ cells/area
infarct volume [mm³]
OPN
placebo

Fig. 2

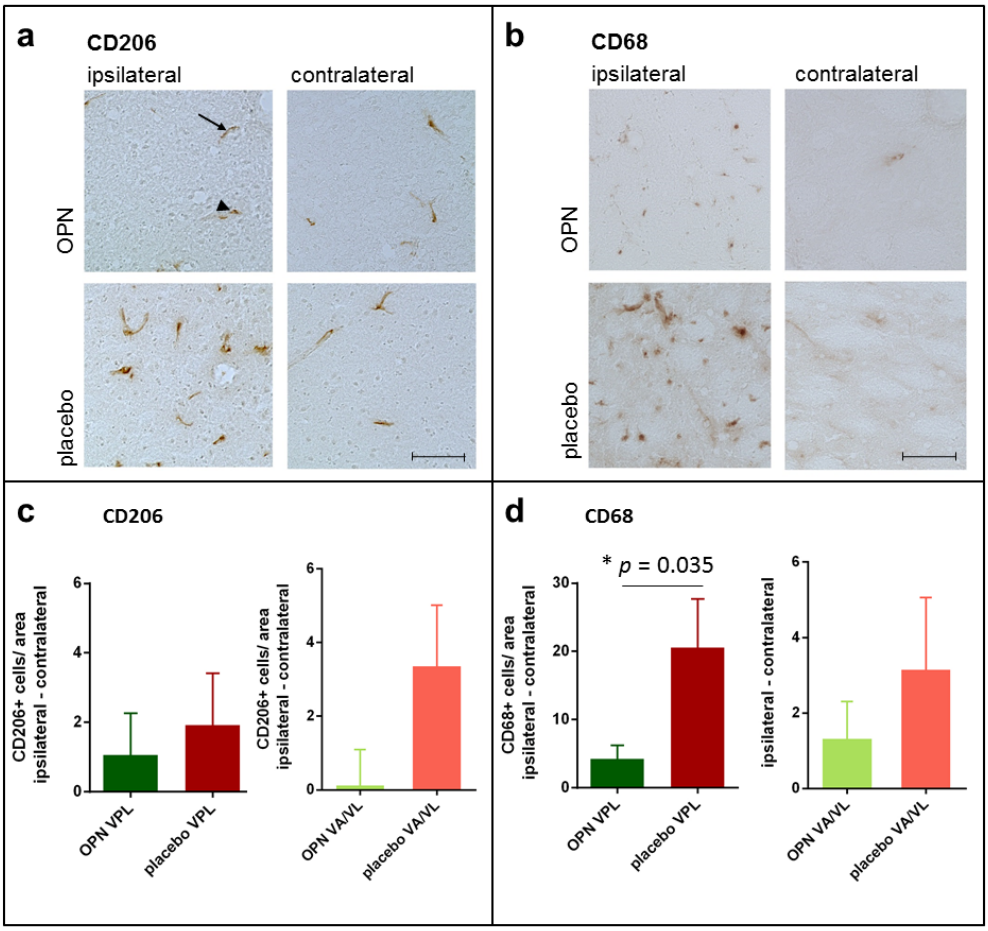
a
CD206
ipsilateral
contralateral
OPN
placebo
b
CD68
ipsilateral
contralateral
OPN
placebo
c
CD206
CD206+ cells/ area
ipsilateral - contralateral
OPN VPL
placebo VPL
OPN VA/VL
placebo VA/VL
d
CD68
* p = 0.035
CD68+ cells/ area
ipsilateral - contralateral
OPN VPL
placebo VPL
OPN VA/VL
placebo VA/VL

Fig.3

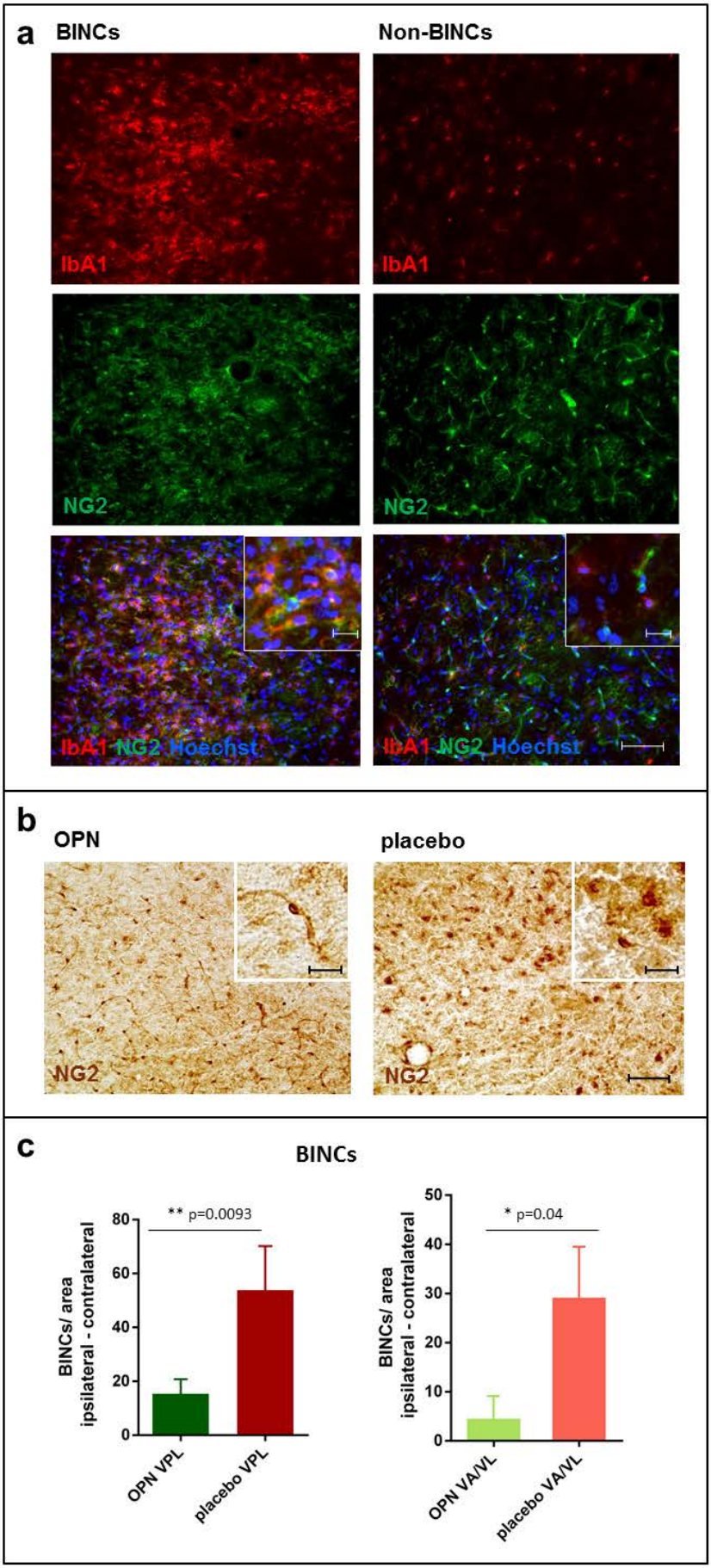
a
BINCs
Non-BINCs
IbA1
IbA1
NG2
NG2
IbA1 NG2 Hoechst
IbA1 NG2 Hoechst
b
OPN
placebo
NG2
NG2
c
BINCs
BINCs/ area ipsilateral - contralateral
** p=0.0093
80
60
40
20
0
OPN VPL
placebo VPL
BINCs/ area ipsilateral - contralateral
* p=0.04
50
40
30
20
10
0
OPN VA/VL
placebo VA/VL

Fig.4

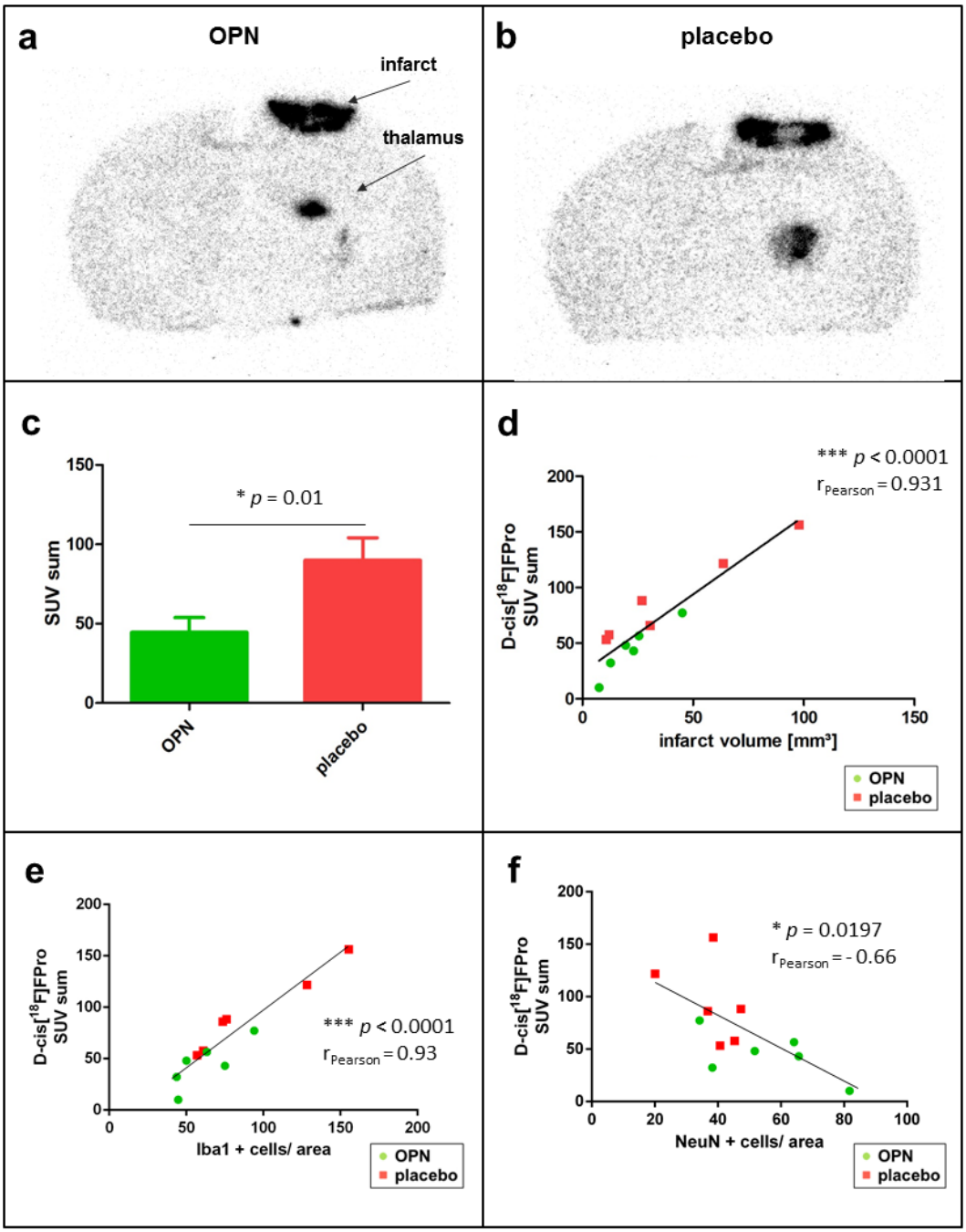
a
OPN
infarct
thalamus
b
placebo
c
SUV sum
* p = 0.01
OPN
placebo
d
*** p < 0.0001
r Pearson = 0.931
D-cis[18F]FPro SUV sum
infarct volume [mm³]
OPN
placebo
e
D-cis[18F]FPro SUV sum
*** p < 0.0001
r Pearson = 0.93
Iba1 + cells/ area
OPN
placebo
f
D-cis[18F]FPro SUV sum
* p = 0.0197
r Pearson = - 0.66
NeuN + cells/ area
OPN
placebo

Fig.5

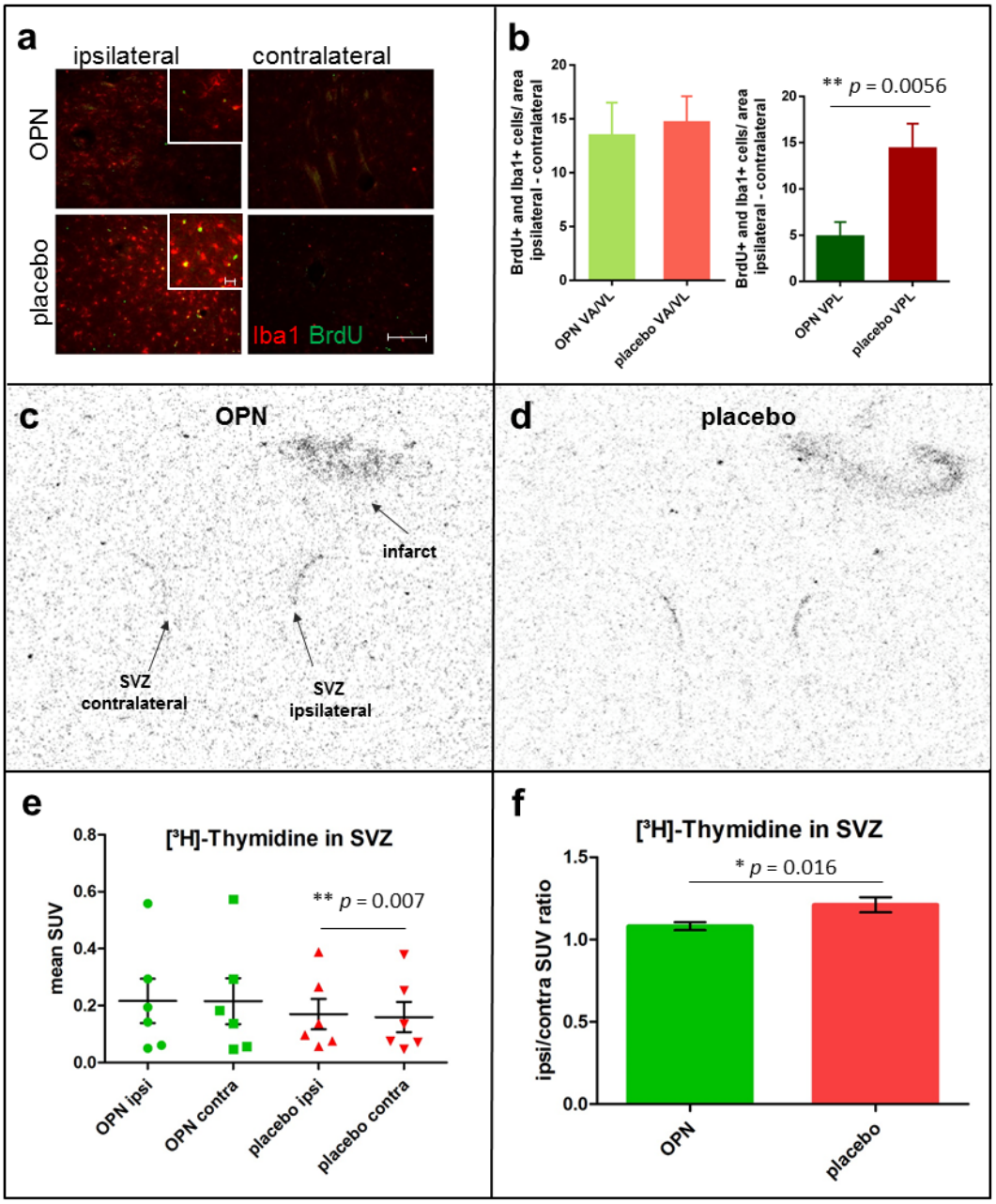
a
ipsilateral
contralateral
OPN
placebo
Iba1 BrdU
b
BrdU+ and Iba1+ cells/ area ipsilateral - contralateral
** p = 0.0056
OPN VA/VL
placebo VA/VL
OPN VPL
placebo VPL
c
OPN
infarct
SVZ contralateral
SVZ ipsilateral
d
placebo
e
[³H]-Thymidine in SVZ
mean SUV
** p = 0.007
OPN ipsi
OPN contra
placebo ipsi
placebo contra
f
[³H]-Thymidine in SVZ
* p = 0.016
ipsi/contra SUV ratio
OPN
placebo

Fig. 6

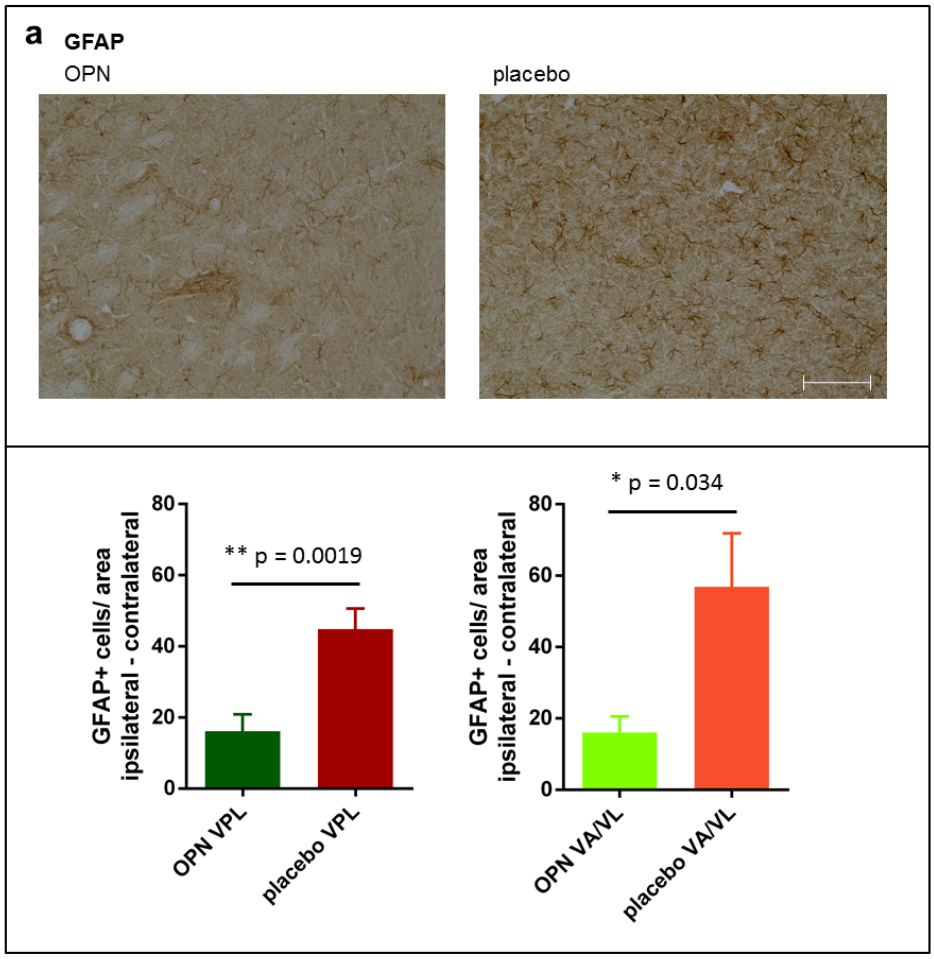
a
GFAP
OPN
placebo
GFAP+ cells/ area ipsilateral - contralateral
** p = 0.0019
OPN VPL
placebo VPL
* p = 0.034
OPN VA/VL
placebo VA/VL
0
20
40
60
80

Fig. 7

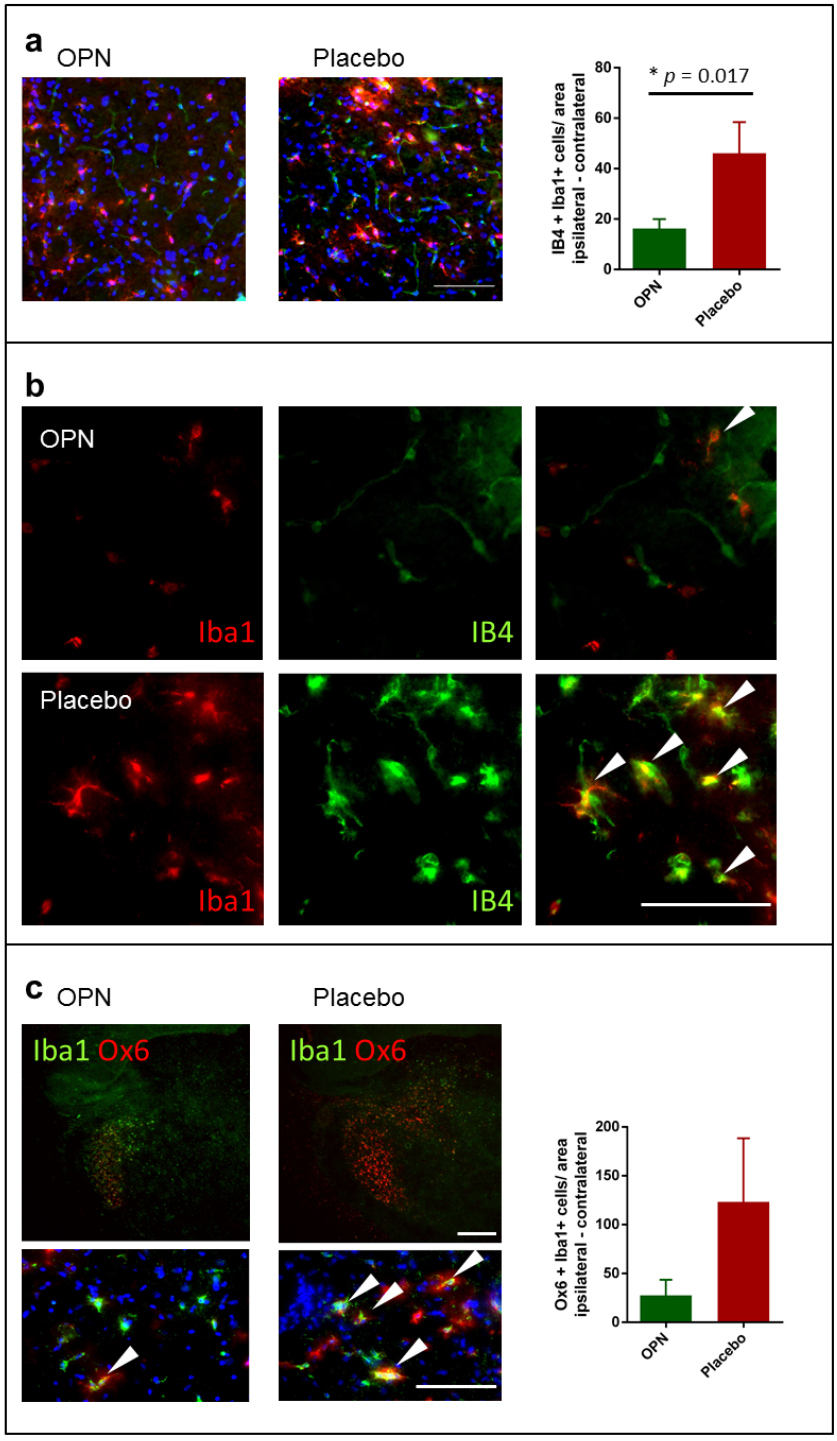
a
OPN
Placebo
* p = 0.017
IB4 + Iba1+ cells/ area
ipsilateral - contralateral
80
60
40
20
0
OPN
Placebo
b
OPN
Iba1
IB4
Placebo
Iba1
IB4
c
OPN
Placebo
Iba1 Ox6
Iba1 Ox6
Ox6 + Iba1+ cells/ area
ipsilateral - contralateral
200
150
100
50
0
OPN
Placebo

Fig. 8